Radiative Ionization Patterns in Cold Precursor of Axisymmetric Detached Shock

ANTHONY N. PIRRI* AND JOSEPH H. CLARKE†
Brown University, Providence, R. I.

Radiative ionization patterns in the precursor of the shock preceding a blunt body immersed in a hypersonic monatomic gas flow are obtained. Based on earlier work that provides for the uncoupling of the radiative transfer and the ionization from the gas dynamics, a plausible model of the shock structure and shock layer radiation is proposed. The rate equation for the production of electrons in the precursor is dependent only upon photon absorption because ionizing and neutralizing collisions are negligible; it is solved in the near precursor where one-step radiative ionization dominates. Geometrical complexities introduced by the multidimensional shock are encountered along with the spectral difficulties associated with nonequilibrium radiative ionization. Spatial calculations for the degree of ionization in argon thoughout the near precursor are presented for a downstream degree of ionization on the stagnation streamline of 0.8, an upstream temperature of 300°K, and an upstream pressure of 10^{-3} atm. Patterns of constant electron density reveal a "concentric sphericity effect" close to the shock axis of symmetry. In addition, asymptotic solutions illustrate the failure of a radiative point source description of the shock layer to yield accurate solutions off the axis of symmetry

I. Introduction

IT is becoming clear that shock precursor ionization is quite common in diverse high-temperature physical phenomena. Historically, the experimental detection of electron precursors to strong shocks has led to much interest in how the hot, often ionized gas behind a shock wave in a tube produces this influence on the cold gas in front. Hollyer[1] first reported precursor electrons in a shock tube, and later Weymann[2] and Gloersen[3] reported the precursor effect. Continued evidence of this phenomenon provided by other experimenters brought about many hypotheses as to the physical mechanisms which caused it. Since the early experiments were designed to measure only electrons, two popular explanations proposed were photoelectric emission due to the radiation from the hot gas upon the shock tube walls, and the diffusion of electrons from behind the shock into the precursor. But, with the use of more sophisticated experimental devices,[4–7] later results tended to support the view that the precursor electrons were due to the photoionization of the cold gas in front of the shock by radiation from the hot shocked gas. Zivanovic[4] and Lederman and Wilson[7] were able to separate the electrons produced by radiation from the diffusing electrons, and they found electrons produced primarily by radiation.

Precursor phenomena have also been observed during the entry of spacecraft and meteoroids into the earth's atmosphere. S. C. Lin,[8] in his interpretation of radar observations made during the re-entry of the first manned Mercury orbital flight, presents evidence of a "photoionization halo" encompassing the spacecraft. The effect of the ionized sheath around bodies on radar echos has recently prompted Marini[9] to study the effect of the enveloping plasma on discrimination during re-entry. Long before the reports of precursor electrons in shock tubes and the observations of Lin, astrophysicists[10,11] using radar to study meteor showers detected an echo associated with the head of a bright meteor. Various explanations of this "meteoric head echo" have been proposed since 1947; however, it was McKinley and Millman[11] in 1949 who hypothesized that it was a "coma of ionization" produced by strong ultraviolet radiation from the meteoroid that caused the reflection. Cook and Hawkins,[12] using the observations of McKinley and Millman, examined this hypothesis and concluded that a precursor "halo" in the shape of a prolate ellipsoid precedes the entering meteoroid.

Concurrent theoretical analysis of precursor ionization is complicated by the coupling of the nonequilibrium collisional and radiative processes with the gas dynamics of the shock structure. The earliest attempts to obtain approximate solutions for electron densities in the precursor of a normal shock were made by Hammerling,[13] Ferrari and Clarke,[14] and Wetzel.[15] Hammerling and Wetzel assumed a priori a precursor uncoupled from the remaining shock structure. Ferrari and Clarke, studying the upstream photoionization as a problem in radiative gas dynamics, discussed the precursor as part of the shock structure utilizing simplified but plausible methods to deal with the transfer of radiation; ultimately, however, they uncoupled the precursor in order to obtain numerical results. Later Clarke and Ferrari[16] studied the nonequilibrium radiative and collisional ionization of a monatomic gas in three spatial dimensions and then placed emphasis on calculating the entire normal shock structure. Utilizing a plausible spectral model they assumed the electrons to be in thermal equilibrium with the atoms and ions, and the dominant ionization to occur directly out of an average state near the ground state (a one-step process). Precursor results were obtained as part of the shock structure, and were used to discuss and assess the accuracy of a black-surface emitter model (BSE). Since a one-step photoionization process may fail to describe the distant ionization of excited atoms actually observed in traditional shock tube experiments, Murty[17] and Dobbins[18] developed more sophisticated monatomic gas models appropriate for higher

Received August 11, 1969; revision received January 8, 1970. This research was sponsored by the Fluid Dynamics Branch of the Office of Naval Research under Contract Nonr 562(35), Requisition NR 061-132, and by the Advanced Research Projects Agency (Ballistic Missile Defense Office). Computer calculations were carried out in part under NSF Grant GJ-409.

* NDEA Fellow and Research Assistant, Division of Engineering and Center for Fluid Dynamics; now Senior Scientist, Avco-Everett Research Laboratory, Everett, Mass. Associate AIAA.

† Professor of Engineering, Division of Engineering and Center for Fluid Dynamics. Associate Fellow AIAA.

upstream pressures than those used in Ref. 16. Using a BSE model for the hot shocked gas, Murty studied the precursor of a normal shock assuming a monatomic and hydrogenic gas with two bound levels and a free level. He also considered the local electron temperature different from the local temperature of the atoms and ions, but this effect on the precursor appears to be unimportant. Dobbins, justifying and utilizing the BSE model for the far ultraviolet radiation, also considered both the one-step and two-step mechanisms, and in addition he included the effect of the walls and the geometry of the cylindrical shock tube.

Interest in the precursor with application to technological re-entry problems has prompted many engineering studies in air. Since the early work of Hammerling, Smith[19] and Edwards[20] have attempted to obtain electron densities in the precursor of a shock preceding a blunt body. Using a simple microscopic model for air, Smith attempted to include three-dimensional effects by modeling the body and shock layer by a point source and calculated velocity, pressure, and density perturbations in addition to electron densities. Edwards utilized a more descriptive microscopic model for air and modeled the shock layer of a blunt body by a constant temperature disk. A constant fraction of the photons absorbed in the precursor was assumed to yield electrons, and with use of a modified BSE model, solutions were obtained for electron densities along the stagnation streamline only.

The motivation for the present work has been 1) the recent study of normal shock waves by Clarke and Onorato,[21] 2) the three-dimensional formulation of Ref. 16, and 3) an interest in analyzing the three-dimensional effects of the curved shock preceding a blunt body and the associated variable temperature shock layer on the cold precursor electron density patterns. Clarke and Onorato consider a monatomic gas initially with two bound levels plus a continuum, and obtain asymptotic solutions for shocks structured by nonequilibrium radiative and collisional ionization. They propose the following "generalized radiation model": asserting that the near precursor is a region where the one-step radiative ionization process is the dominant mechanism, and the far precursor is a region where the two-step ionization mechanism dominates, they ultimately divide the disparate radiative mechanisms into complete inner and outer shocks and propose that the separated solutions can be matched asymptotically; their absorption spectrum consists of a bar-type line augmented by wings along with the two continuum bound-free spectrum. For calculation of the inner shock when $p_1 \leq 10^{-3}$ atm (where subscript 1 denotes freestream conditions), the outer shock is weak and is neglected. In addition, it is assumed and verified a posteriori that, with sufficient triggering precursor ionization and for flow conditions of interest, the nonequilibrium electron-atom collisional reactions take place in a boundary layer directly behind the embedded shock that is thin enough to be transparent with respect to the one-step process. In this boundary layer these collisions rapidly bring the degree of ionization to a condition of local thermodynamic equilibrium (LTE). This threefold layering of the radiative and collisional mechanisms couples with the emergence of a rather small emission-convection ratio for the flow conditions studied to yield great simplifications. The small ratio leads to an expansion that to lowest order gives the BSE model for the tail; higher-order corrections are also obtained as a function of only the downstream equilibrium conditions; therefore, for the conditions examined, a rational uncoupling of the precursor from the remaining tail shock structure emerges. This in turn provides a basis for the study of more complex problems, for then the shock structure is no longer needed to obtain the precursor electron densities. Provided the flow conditions are maintained in the range studied in Ref. 21, this precursor uncoupling plus the justifiable neglect of local emission and inelastic collisions in the cold precursor[21] make a study of the multidimensional precursor both possible and inviting.

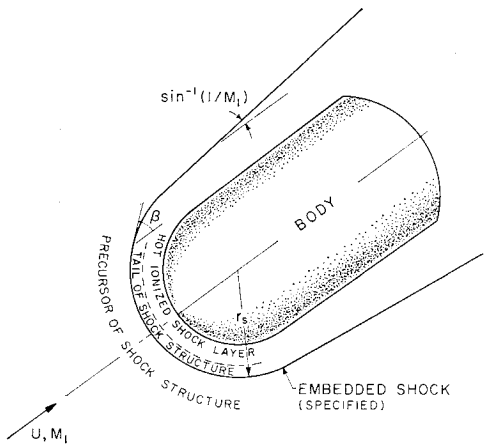

Fig. 1 Sketch of problem.

The three-dimensional effects of the curved shock preceding a blunt body and the variable temperature just behind the shock on the spatial radiation and electron densities in the precursor are presented in the present paper. A monatomic gas and the same range of flow conditions used by Clarke and Onorato are maintained in order to remain within the rationale of their radiation model and shock morphology, consisting mainly of the collisional boundary layer and the BSE model of the tail. The use of a monatomic gas simplifies the analysis so greater understanding of the three-dimensional effects is possible. The microscopic and macroscopic models of Refs. 16 and 21 are retained without the spectral simplification called case 1, and the primary region of interest is the near precursor where the one-step radiative ionization mechanism is dominant.

The shape of the embedded shock is specified as spherical out to where the shock wave angle β is equal to the Mach angle (see Fig. 1). The corresponding body shape could be found by utilizing techniques developed for solving the "inverse problem" of hypersonic gas dynamics. Since the precursor will weaken as the wave angle decreases away from the shock axis of symmetry, the thin collisional boundary-layer assumption and the BSE assumption for the shock layer enveloping the body surface (c.f. Fig. 1) will deteriorate quite abruptly as viable descriptions when the wave angle approaches a certain value. But it will be seen from the numerical results that, when the requirements for the BSE and the thin collisional boundary layer are no longer satisfied, the shock layer is then no longer hot enough to contribute sensibly to the radiative ionization of the precursor. The addition of curvature to the shock introduces an additional characteristic length, the radius of the embedded shock r_s. The dimensionless geometric parameter τ_{s1} then is the ratio of the radius r_s to the freestream photon mean free path evaluated at the edge frequency, λ_{j1}; thus $\tau_{s1} = r_s\lambda_{j1}^{-1}$. Restrictions on this parameter τ_{s1} are necessary to maintain the BSE description of the shock layer in the presumed presence of the body behind the shock. Proper sizing is necessary to prevent the body surface from truncating the thin collisional layer or the nonequilibrium tail of the enveloping shock structure. In addition, because the flow will stream around the body after passing through the structured shock with resulting changes in fluid dynamical variables, the shock layer as measured by the shock detachment distance must be sufficiently thick optically so that a BSE description at the local equilibrium shock temperature (T_4) just behind the embedded shock structure will suffice to model the radiation that penetrates into the precursor. For the purpose of calculating T_4, the structured equilibrium

shock can be replaced by a hemispherical discontinuity radiating locally like a BSE.

II. Formulation

The nonequilibrium ionization-rate equation, the equation of radiative transfer, and the associated gasdynamical relations are the equations necessary to describe the ionization by radiation in the cold precursor of a shock preceding a blunt body. We assume a singly ionizable monatomic gas, no inelastic collisions, and negligible emission (radiative recombination); the rate equation for the electron production in the precursor can be written directly in terms of the divergence of a photon particle flux vector. From Ref. 16 this equation becomes

$$\rho \frac{D\alpha}{Dt} = -m_a \nabla \cdot \int_{\nu_j}^{\infty} (h\nu)^{-1} \mathbf{F}_\nu d\nu \tag{2.1}$$

where α is the degree of ionization defined respectively in terms of the number densities of atoms, ions, and electrons, n_a, n_i, and $n_e = n_i$ as $\alpha = n_e/(n_a + n_i)$; ρ is the density of the gas mixture; m_a is the mass of an atom; h is Planck's constant; ν_j is the first edge frequency; and $\mathbf{F}_\nu$ is the spectral radiative flux vector. Since only one-step ionization is considered, only photons with energy $h\nu \geq h\nu_j$ will contribute to the production of electrons. The explicit equation of radiative transfer in the precursor is simplified considerably with negligible radiative recombination since the nonequilibrium source term in Eq. (9.1a) of Ref. 16 drops out, and the only radiative process taking place is absorption. This equation can then be written along a generic ray of radiation as

$$\partial I_\nu / \partial s = -\rho(1 - \alpha)\kappa_\nu I_\nu \tag{2.2}$$

where I_ν is the specific intensity of radiation, s is the intrinsic ray coordinate measured from the shock to the influenced point, and κ_ν is the absorption coefficient per unit mass of atoms equal to[16] $\kappa\nu^{-2}$ (where $\kappa \equiv hm_a^{-1}C_{ir}^{-1}\nu_j^{-2} = \text{const}$ and C_{ir} is defined in Ref. 16). The volumetric absorption coefficient at $\nu = \nu_j$ is $\rho(1 - \alpha)\kappa \equiv \lambda_j^{-1}$. Equation (2.2) can be formally solved along a ray and the solution for I_ν at the generic influenced point s becomes

$$I_\nu(s) = I_\nu(s = 0) \exp\left[-\int_0^s \rho'(1 - \alpha')\kappa_\nu' ds' \right] \tag{2.3}$$

where prime denotes variables at the elemental ray ds'. Since every ray originates behind the shock, the BSE model of the shock tail structure yields

$$I_\nu(s = 0) = B_\nu(T_4) \tag{2.4}$$

where $B_\nu(T_4)$ is the Planck function evaluated at the local downstream equilibrium shock temperature. Utilizing Eqs. (2.2–2.4) along with the traditional derivation of the divergence of the spectral radiative flux vector in terms of the specific intensity,[22] we obtain

$$\nabla \cdot \mathbf{F}_\nu = -\rho(1 - \alpha)\kappa_\nu \int_{4\pi} B_\nu(T_4) \exp\left[-\int_0^s \rho'(1 - \alpha')\kappa_\nu' ds' \right] d\omega \tag{2.5}$$

where $d\omega$ is an element of solid angle subtended by a ray of radiation.

Associated with the preceding equations of rate and radiation are the gas-dynamical relations for the flow in the precursor. With transport effects neglected, the steady-flow equations of continuity, momentum and energy are, respectively,

$$\nabla \cdot (\rho \mathbf{V}) = 0 \tag{2.6}$$

$$\nabla \cdot (\rho \mathbf{V}\mathbf{V}) = -\nabla p \tag{2.7}$$

$$\nabla \cdot [\rho \mathbf{V}(V^2/2 + E + p/\rho)] = -\nabla \cdot \mathbf{F} \tag{2.8}$$

where $\mathbf{V}$ is velocity, p is pressure, E is internal energy per unit mass of mixture, and $\mathbf{F}$ is the radiative flux vector defined for the one-step mechanism by

$$\mathbf{F} = \int_{\nu_j}^{\infty} \mathbf{F}_\nu d\nu \tag{2.9}$$

The gas mixture is one of perfect gases and the thermal and caloric equations of state are[16]

$$p = \rho RT(1 + \alpha) \tag{2.10}$$

$$E = \tfrac{3}{2}RT(1 + \alpha) + E_e + \alpha RT_j \tag{2.11}$$

where R is the gas constant per unit mass of the atoms, E_e is the electronic energy of the atoms and ions, T_j is the ionization temperature, and T is the translational temperature, which for the single-temperature model is common among the species. E_e can be neglected in the precursor.

With a normalization similar to that of Ref. 21, the governing Eqs. (2.1, 2.5, and 2.6–2.11) are nondimensionalized in the following way:

$$\hat{T} = \frac{T}{T_j}; \quad \hat{\rho} = \frac{(RT_j)^{1/2}}{G}\rho; \quad \hat{V} = \frac{V}{(RT_j)^{1/2}}$$
$$\hat{\nu} = \frac{\nu}{\nu_j}; \quad \hat{B}_\nu = \frac{B_\nu \nu_j}{GRT_j}; \quad \hat{p} = \frac{p}{G(RT_j)^{1/2}}; \quad \hat{E} = \frac{E}{RT_j} \tag{2.12}$$
$$\hat{s} = \frac{s}{r_s}; \quad \hat{\nabla} = r_s \nabla; \quad \hat{F} = \frac{F}{GRT_j}$$

Here G is the freestream mass flow and r_s is the radius of the embedded shock. Using Eq. (2.12), we obtain for the relevant equations governing the nonequilibrium precursor phenomena

$$\hat{\rho}\hat{\mathbf{V}} \cdot \hat{\nabla}\alpha = -\int_1^{\infty} \hat{\nu}^{-1} \hat{\nabla} \cdot \hat{\mathbf{F}}_\nu d\hat{\nu} \tag{2.13}$$

$$\hat{\nabla} \cdot \hat{\mathbf{F}}_\nu = -\tau_s \hat{\nu}^{-2} \int_{4\pi} \hat{B}_\nu(\hat{T}_4) \exp\left[-\int_0^{\hat{s}} \tau_s' \hat{\nu}^{-2} d\hat{s}' \right] d\omega \tag{2.14}$$

$$\hat{\nabla} \cdot (\hat{\rho}\hat{\mathbf{V}}) = 0 \tag{2.15}$$

$$\hat{\nabla} \cdot (\hat{\rho}\hat{\mathbf{V}}\hat{\mathbf{V}}) = -\nabla p \tag{2.16}$$

$$\hat{\nabla} \cdot \{\hat{\rho}\hat{\mathbf{V}}[\hat{V}^2/2 + \alpha(1 + \tfrac{5}{2}\hat{T}) + \tfrac{5}{2}\hat{T}]\} = \hat{\nabla} \cdot \hat{\mathbf{F}} \tag{2.17}$$

$$\hat{p} = \hat{\rho}\hat{T}(1 + \alpha) \tag{2.18}$$

It should be noted that $\tau_s \equiv r_s/\lambda_j$ is a variable at this point since λ_j is the local photon mean free path in the precursor.

It would be extremely difficult to solve simultaneously Eqs. (2.13–2.18) in their present form because of their nonlinearity, multidimensionality, and spectral aspect. Moreover, it is natural to utilize simplifications which arise for the actual flow conditions of interest. A measure of the strength of the spectral radiation emitted from the shock tail is $\hat{B}_\nu(\hat{T}_4)$;

$$\hat{B}_\nu(\hat{T}_4) = \Lambda_E \hat{\nu}^3 [\exp(\hat{\nu}/\hat{T}_4) - 1]^{-1} \tag{2.19}$$

where

$$\Lambda_E = 2k^3 T_j^3 c^{-2} h^{-3} m_a G^{-1} \tag{2.20}$$

It is found from numerical calculations that $\hat{B}_\nu(\hat{T}_4)$ over the frequency range ν_j to ∞ as well as the two indicated spectral integrals of $\hat{B}_\nu$ are very small quantities. Therefore, as in Ref. 21, the radiative ionization in the precursor is studied under the mathematical limit

$$\Lambda_E \to 0 \tag{2.21}$$

From Eqs. (2.9, 2.14, and 2.19) it can be seen that the right sides of the rate equation (2.13) and the energy equation (2.17) are $\sim\Lambda_E$. In the energy equation Λ_E can be considered to play the mathematical role of the standard equilibrium emission-convection ratio. With the precursor

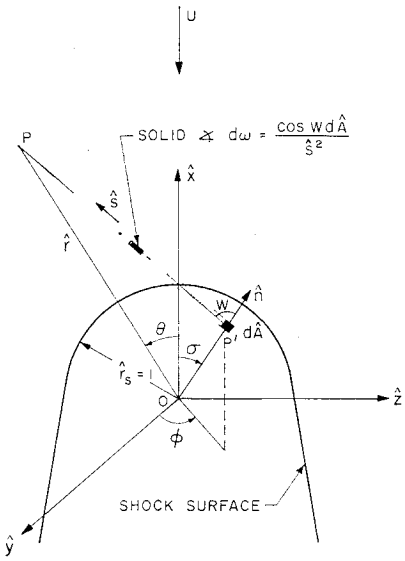

Fig. 2 Geometry.

mass flow and kinetic energy ~1, the absorption of radiation can be neglected in the energy equation to lowest order under the limit (2.21). In the rate equation the ordering of the right side along with the boundary condition that $\alpha \to 0$ at ∞ means that $\alpha \sim \Lambda_E$. Therefore, under the limit (2.21), it is implied in the precursor that

$$\alpha \ll 1 \tag{2.22}$$

and, furthermore,

$$\hat{V}^2/2 \gg \alpha(1 + \tfrac{5}{2}\hat{T}) \tag{2.23}$$

in Eq. (2.17). The preceding discussion demonstrates that, under the limit Eq. (2.21), all the terms which couple the radiative ionization to the gas dynamics [in Eqs. (2.15–2.18)] will drop out to lowest order. With no sensible upstream radiative influence, it therefore follows that the gas dynamic variables $\hat{p}$, $\hat{\rho}$, $\hat{T}$, and $\hat{V}$ remain constant in the precursor at the freestream value. It is then necessary first to evaluate the expression for the divergence of the spectral radiative flux vector Eq. (2.14), and then solve the rate Eq. (2.13) in order to obtain the electron number densities in the precursor.

Simplifications which emerge from the rational uncoupling of the gas dynamics from the nonequilibrium radiative ionization are 1) the parameter $\tau_s = \tau_{s1} = \text{const}$ (c.f. Sec. I), since now $\lambda_j = \lambda_{j1}$, and Eq. (2.14) simplifies especially because the integral over distance becomes proportional to distance; 2) $\hat{\rho}\hat{\mathbf{V}}$ in Eq. (2.13) becomes $\hat{\rho}_1\hat{\mathbf{U}}$ and uniform, and 3) the smallness of Λ_E implies that the precursor and outer[21] tail of the shock structure will be weak from the gas dynamic point of view, although the precursor is still of notable physical and observational significance. Therefore, for the purpose of actual calculation[23] of $\hat{T}_4$ from Rankine-Hugoniot equilibrium oblique shock relations, the equilibrium shock can be regarded as geometrically identical to the embedded shock.

III. Solution for $\hat{\nabla}\cdot\hat{\mathbf{F}}_\nu$

With the simplification afforded by the uncoupling of the radiation, the expression for the divergence of the spectral radiative flux vector Eq. (2.14) becomes

$$\hat{\nabla}\cdot\hat{\mathbf{F}}_\nu = -\tau_{s1}\hat{\nu}^{-2}\int_{4\pi}\hat{B}_\nu(\hat{T}_4)\exp[-\tau_{s1}\hat{\nu}^{-2}\hat{s}]d\omega \tag{3.1}$$

Before the preceding integral can be evaluated it is necessary to establish a reference coordinate system and introduce the geometry of the problem. In Fig. 2 a standard spherical coordinate system has been centered at O; P is the influenced point, P' is the influencing point, and $d\omega$, the solid angle subtended by a ray of radiation s through P, is written in terms of the area and the normal to the shock surface. Using ancillary geometrical relations between the distances and angles specified in Fig. 2, we can write for $\hat{\nabla}\cdot\hat{\mathbf{F}}_\nu$

$$\hat{\nabla}\cdot\hat{\mathbf{F}}_\nu = \tau_{s1}\hat{\nu}^{-2}\int_{\phi_1}^{\phi_2}\int_{\sigma_1}^{\sigma_2}\frac{\hat{B}_\nu(\hat{T}_4)(1-\hat{r}\cos\Omega)\exp[-\tau_{s1}\hat{\nu}^{-2}(\hat{r}^2+1-2\hat{r}\cos\Omega)^{1/2}]\sin\sigma d\sigma d\phi}{(\hat{r}^2+1-2\hat{r}\cos\Omega)^{3/2}} \tag{3.2}$$

where $\cos\Omega = \cos\theta\cos\sigma + \sin\theta\sin\sigma\cos\phi$, and $\hat{T}_4 = \hat{T}_4(\sigma)$ only, because the shock is symmetric about the x axis. The limits of integration ϕ_1, ϕ_2, σ_1, σ_2 are found from a consideration of the line-of-sight property of a ray of radiation. Analytic expressions for these limits will depend upon the location of the influenced point relative to the shock surface (see Fig. 3). When $\hat{r} > 1/\cos\theta$, $\phi_1 = 0$ and $\phi_2 = \pi$; when $\hat{r} = 1/\cos\theta$, $\phi_1 = -\pi/2$ and $\phi_2 = \pi/2$; when $\hat{r} < 1/\cos\theta$,

$$\begin{aligned}\phi_1 &= -\cos^{-1}[(1-\hat{r}^2\cos^2\theta)^{1/2}/\hat{r}\sin\theta]\\ \phi_2 &= \cos^{-1}[(1-\hat{r}^2\cos^2\theta)^{1/2}/\hat{r}\sin\theta]\end{aligned} \tag{3.3}$$

For the limits σ_1 and σ_2, we obtain

$$\tan\sigma_{1,2} = \frac{\hat{r}^2\sin\theta\cos\theta\cos\phi \mp [\hat{r}^2(\cos^2\theta + \sin^2\theta\cos^2\phi) - 1]^{1/2}}{1-\hat{r}^2\sin^2\theta\cos^2\phi} \tag{3.4}$$

In Fig. 3 the shaded area of the shock surface indicates the amount of the radiating shock that contributes to photon absorption at the influenced point P. In terms of the rays that pass through this point, the radiation at P is highly nonisotropic. However, the total amount of radiation absorbed per unit volume per unit time per unit frequency will be symmetric about the x axis, i.e., $\hat{\nabla}\cdot\hat{\mathbf{F}}_\nu = \hat{\nabla}\cdot\hat{\mathbf{F}}(\hat{r},\theta)$.

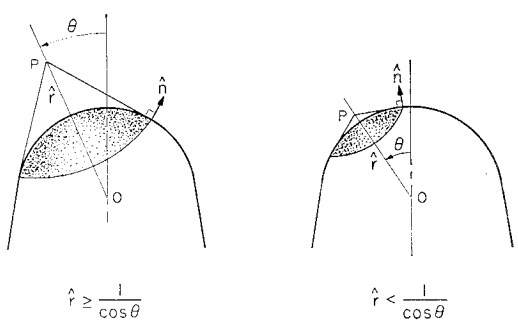

Fig. 3 Geometry: limits of radiative influence.

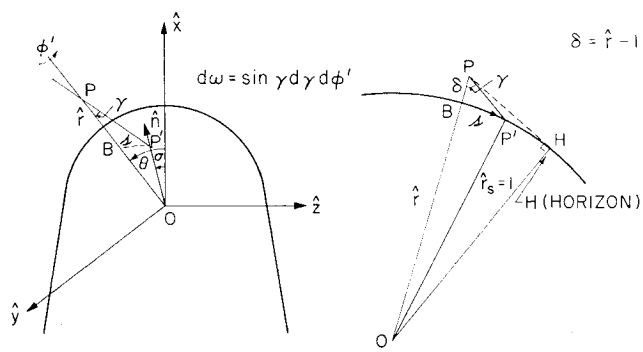

Fig. 4 Geometry: influence for $\hat{r} - 1 \ll 1$.

In addition, the angle σ is related to the shock angle through the geometrical relation $\sigma = \pi/2 - \beta$. When the upper limit of radiation influence, σ_2, exceeds $\pi/2$ minus the Mach angle [$\sigma_2 > \pi/2 - \sin^{-1}(1/M_1)$], the corresponding element of the influencing shock is no longer a discontinuity and is no longer spherical. It can be shown, however, that when this situation arises, the temperature $\hat{T}_4$ corresponding to $\sigma_2 = \pi/2 - \sin^{-1}(1/M_1)$ is so small ($\hat{T}_4 = \hat{T}_1 \ll 1$ at this point) that the gas behind the wave no longer emits radiation. Therefore, the upper limit of radiative influence σ_2 can be restricted to $\sigma_2 \leq \pi/2 - \sin^{-1}(1/M_1)$ without any loss of generality.

From Eqs. (3.2, 3.3, and 3.4) it can be seen that when $\hat{r} \to 1$, i.e., the influenced point approaches the shock surface, $\sigma_1 \to \sigma_2$, and the integrand also becomes singular at a distinct value of Ω. Thus, the integration of Eq. (3.2) becomes indeterminate, and to avoid numerical difficulties close to the surface it is necessary to seek an asymptotic solution for $\hat{\nabla}\cdot\hat{\mathbf{F}}_\nu$ for ($\hat{r} - 1) \ll 1$. The difficulty arises when $(\hat{r} - 1) \ll 1$ for which the shock surface appears planar to an observer at the influenced point, and, since the radiation is line-of-sight, the behavior of Eq. (3.2) is extremely sensitive with the reference spherical coordinate system located at O. To avoid this difficulty when $(\hat{r} - 1) \ll 1$, an intrinsic coordinate system is established at the influenced point P. The geometry associated with this new coordinate system is shown in Fig. 4. In terms of this coordinate system at P, the elemental solid angle $d\omega = \sin\gamma d\gamma d\phi'$; an additional coordinate $\mathcal{S}$ is defined along the shock surface and $\delta \equiv \hat{r} - 1$; relating the appropriate quantities geometrically, we find for Eq. (3.1)

$$\hat{\nabla}\cdot\hat{\mathbf{F}}_\nu = -\tau_{s1}\hat{\nu}^{-2}\int_{4\pi}\hat{B}_\nu(\hat{T}_4)\exp\{-\tau_{s1}\hat{\nu}^{-2}[\hat{r}\cos\gamma - (1 - \hat{r}^2\sin^2\gamma)^{1/2}]\}\sin\gamma d\gamma d\phi' \quad (3.5)$$

It is necessary to obtain an expansion for $\hat{B}_\nu[\hat{T}_4(\sigma)]$ when $\delta \ll 1$ in terms of the current integration parameters before Eq. (3.5) can be evaluated asymptotically for $\delta \to 0$. With $\delta \ll 1$, it can be seen in Fig. 4 that $\tan\gamma \approx \mathcal{S}/\delta$ and the segment of the shock surface that influences P will be in the close vicinity of point B. Therefore, $\hat{B}_\nu$ will be expanded about point B, i.e. $\mathcal{S} = 0$. From the geometry, $\hat{B}_\nu[\hat{T}_4(\sigma)]_{\mathcal{S}=0} = \hat{B}_\nu[\hat{T}_4(\sigma)]_{\sigma=\theta}$ and

$$d^n\hat{B}_\nu/d\mathcal{S}^n = (-1)^n \sin^n\phi' d^n\hat{B}_\nu/d\sigma^n$$

for any integer n. The expansion for $\hat{B}_\nu(\hat{T}_4)$ about $\mathcal{S} = 0$ then becomes

$$\hat{B}_\nu(\hat{T}_4) = \hat{B}_\nu(\hat{T}_4)_{\sigma=\theta} - \sin\phi'\left(\frac{d\hat{B}_\nu}{d\sigma}\right)_{\sigma=\theta}\delta\tan\gamma + \frac{\sin^2\phi'}{2}\times\left(\frac{d^2\hat{B}_\nu}{d\sigma^2}\right)_{\sigma=\theta}\delta^2\tan^2\gamma + \ldots \quad (3.6)$$

Substituting Eq. (3.6) into Eq. (3.5) and integrating term by term we obtain for $\delta \to 0$

$$\hat{\nabla}\cdot\hat{\mathbf{F}}_\nu = \left[-2\pi\tau_{s1}\hat{\nu}^{-2}\hat{B}_\nu(\hat{T}_4)_{\sigma=\theta} + \frac{\pi}{2}\tau_{s1}\hat{\nu}^{-2}\delta^2\left(\frac{d^2\hat{B}_\nu}{d\sigma^2}\right)_{\sigma=\theta}\right]\times\left\{\exp(-\tau_{s1}\hat{\nu}^{-2}(2\delta)^{1/2})\left[\frac{1-\delta}{2\tau_{s1}\hat{\nu}^{-2}} - (1-\delta)\left(\frac{\delta}{2}\right)^{1/2}\right] + \exp(-\tau_{s1}\hat{\nu}^{-2}\delta)\left[(1-\delta) - \frac{1-\delta}{2\tau_{s1}\hat{\nu}^{-2}}\right] + \tau_{s1}\hat{\nu}^{-2}\delta\times\{E_1[\tau_{s1}\hat{\nu}^{-2}(2\delta)^{1/2}] - E_1(\tau_{s1}\hat{\nu}^{-2}\delta)\} + \Pi_1 - \Pi_2 + O(\tau_{s1}^2\delta^4)\right\} \quad (3.7)$$

where

$$\Pi_1 = \int_\delta^{(2\delta)^{1/2}} z^2(z^2 + 2\delta)^{-2}\exp(-\tau_{s1}\hat{\nu}^{-2}z)dz$$

$$\Pi_2 = \int_\delta^{(2\delta)^{1/2}} 2\delta(z^2 + 2\delta)^{-2}\exp(-\tau_{s1}\hat{\nu}^{-2}z)dz$$

For most of the calculations performed in this paper, Eq. (3.2) was used to obtain the divergence of the spectral radiative flux vector. For close results ($\delta \ll 1$), Eq. (3.7) was utilized. No formal asymptotic matching of the solutions was attempted but the point at which numerical difficulties were encountered with Eq. (3.2) was determined from a careful examination of the numerical results.

IV. Solution for Degree of Ionization

Once the divergence of the spectral radiative flux vector has been evaluated, the remaining rate equation must be solved to determine the degree of ionization. Equation (2.13) is a differential equation of the form

$$\hat{\rho}_1\hat{\mathbf{U}}\cdot\hat{\nabla}\alpha = G(\hat{r},\theta) \quad (4.1)$$

In spherical coordinates this equation becomes an inhomogeneous first-order partial differential equation with coefficients $-\hat{\rho}_1\hat{U}\cos\theta$ and $\hat{\rho}_1\hat{U}\hat{r}^{-1}\sin\theta$. There are techniques for solving such an equation using its respective characteristic equations;[24] however, by a simple transformation to cartesian coordinates, Eq. (4.1) can be integrated directly. Since the freestream velocity vector is along the x axis, and the boundary condition on α is $\alpha \to 0$ as $x \to \infty$, the transformation permits quadrature in Eq. (4.1). Substituting (3.2) into (2.13), transforming to cartesian coordinates, integrating, and transforming back to spherical coordinates, we find

$$\alpha = \frac{\tau_{s1}}{\hat{\rho}\hat{U}}\int_{\hat{r}}^\infty\int_1^\infty\int_{\phi_1}^{\phi_2}\int_{\sigma_1}^{\sigma_2}\frac{\hat{\nu}^{-3}\hat{B}_\nu\exp\{-\tau_{s1}\hat{\nu}^{-2}(\eta^2 + 1 - 2\eta\cos\Omega)^{1/2}\}(\eta\cos\Omega - 1)\sin\sigma\, d\sigma\, d\phi\, d\hat{\nu}\, d\eta}{(\eta^2 + 1 - 2\eta\cos\Omega)^{3/2}(1 - \hat{r}^2\eta^{-2}\sin^2\theta)^{1/2}} \quad (4.2)$$

$$\cos\Omega = \cos\theta\cos\sigma + \sin\theta\sin\sigma\cos\phi$$

$$\hat{B}_\nu = \hat{B}_\nu(\hat{T}_4),\ \hat{T}_4 = \hat{T}_4(\sigma),\ \alpha = \alpha(\hat{r},\theta)$$

$$\sigma_1 = \sigma_1(\eta,\theta,\phi),\ \sigma_2 = \sigma_2(\eta,\theta,\phi)$$

When $\hat{r} - 1 \ll 1$, Eq. (3.7) is substituted into Eq. (2.13) and the resulting integration is carried out from $\hat{r}$ to $\hat{r}^*$, where $\hat{r}^*$ is the point at which Eq. (3.7) breaks down. Thereafter, Eq. (4.2) is utilized with $\hat{r}$ replaced by $\hat{r}^*$. The numerical results from these two operations are then added to obtain α at $(\hat{r},\theta)$. The two innermost integrations in Eq. (4.2) are the geometrical integrations associated with the evaluation of $\hat{\nabla}\cdot\hat{\mathbf{F}}_\nu(\eta,\theta)$, the next is the spectral integration, and the last can be viewed as a streamline integration to obtain $\alpha(\hat{r},\theta)$. The common frequency-distance coupling of radiative gas dynamics is apparent in Eq. (4.2). In Ref. 16 a spectral simplification that implements the frequency integration is presented as case 1; in general, no simplification can be introduced here because of the geometrical complexities. But, for large distances, it will be shown in the next section that the frequency integration can be performed once a dominant ionizing frequency is identified.

V. Asymptotic Representation of Solution for Large Distances

The expression for the degree of ionization, Eq. (4.2), can only be evaluated numerically for general $\hat{r}$ and θ. However, for $\hat{r} \to \infty$, an asymptotic representation of Eq. (4.2) can be obtained that provides insight into the behavior of the patterns for $\hat{\nabla}\cdot\hat{\mathbf{F}}_\nu$ and α at large distances. For $\hat{r} \to \infty$, Eq.

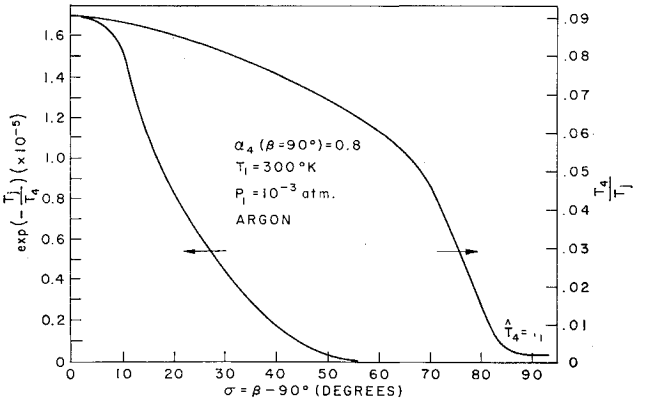

Fig. 5 Local equilibrium shock temperature.

(3.2) becomes

$$\hat{\nabla}\cdot\hat{\mathbf{F}}_\nu \sim \left[-\tau_{s1}\hat{\nu}^{-2}\int_{\phi_1}^{\phi_2}\int_{\sigma_1}^{\sigma_2}\hat{B}_\nu(\hat{T}_4)\cos\Omega\times \sin\sigma\exp(\tau_{s1}\hat{\nu}^{-2}\cos\Omega)d\sigma d\phi\right]\frac{\exp(-\tau_{s1}\hat{\nu}^{-2}\hat{r})}{\hat{r}^2} \quad (5.1)$$

The bracketed term for large distance becomes independent of $\hat{r}$ but displays no simple dependence on θ. If the θ dependence were to be ignored, it can be shown that the remaining expression is then the solution for $\hat{\nabla}\cdot\hat{\mathbf{F}}_\nu$ at the influenced point P due to a radiating point source at O. Thus, Eq. (5.1) can be considered the solution for a radiating point source modified by a significant angular dependent strength. Utilizing Eq. (5.1) for $\hat{\nabla}\cdot\hat{\mathbf{F}}_\nu$ and standard asymptotic techniques successively on the remaining integrals,[23] we obtain for Eq. (4.2) as $\hat{r}\to\infty$

$$\alpha = \frac{\tau_{s1}\Lambda_E}{2\hat{\rho}_1\hat{U}\hat{r}}\left(\frac{\pi}{3}\right)^{1/2}\int_{\phi_1}^{\phi_2}\int_{\sigma_1}^{\sigma_2}(2\hat{T}_4)^{2/3}(\tau_{s1}\hat{r}')^{1/6}\exp(-3W\hat{r}'\hat{r}^{-1})\sin\sigma\cos\Omega\cdot\left[\left(\frac{1}{W+2}+\frac{2}{(W+2)^3}\right)+\sum_{j=1}^{N}C_j\left(\frac{1}{W+2(j+1)}+\frac{2(j+1)}{[W+2(j+1)]^3}\right)+O\left(\frac{1}{[W+2(N+2)]}\right)\right]d\sigma d\phi \quad (5.2)$$

where

$$\hat{r}' = \hat{r}-\cos\Omega,\quad W=(\tau_{s1}\hat{r}^3\hat{r}'^{-2})^{1/3}(2\hat{T}_4)^{-2/3}$$

and

$$C_j=\prod_{j=0}^{j-1}(2i+1)\left[\prod_{i=1}^{j}2i\right]^{-1}(\sin\theta)^{2j}$$

The spectral integration has been accomplished by using the method of steepest descents to isolate the dominant ionizing frequency and obtain the maximum contribution to the integral. It is found, for large distances, that the dominant frequency $\hat{\nu}_0$ is not the edge frequency but, is coupled to distance. For the $\hat{\nu}^{-2}$ dependence of the absorption coefficient utilized in this paper, the dominant ionizing frequency is located at $\hat{\nu}_0=(2\tau_{s1}\hat{r}\hat{T}_4)^{1/3}$. Thus, the greater the distance the greater the dominant frequency becomes. The importance of the extreme ultraviolet region is further illuminated if a hat-type frequency model of the true absorption spectrum (for argon, say) is employed: no absorption for $0\le\nu\le\nu_j$ and $\nu^*\le\nu\le\infty$ and constant absorption for $\nu_j\le\nu\le\nu^*$. Because the contribution from the exact absorption spectrum from ν^* to ∞ is not accounted for, a hat-type model will clearly[25] underestimate the number of photons absorbed for sufficiently large distances due to the dependence on distance of the dominant frequency.

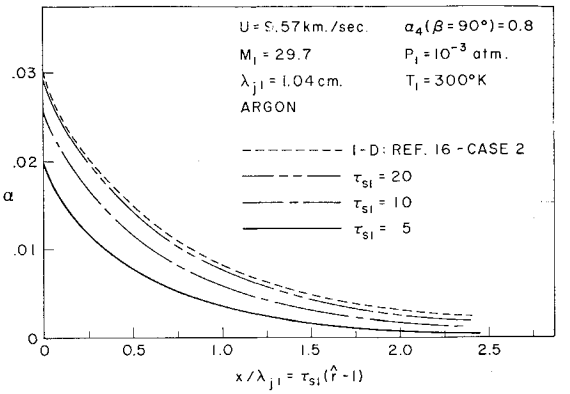

Fig. 6 Degree of ionization α vs optical distance (x/λ_{j1}) in precursor: $\theta=0$.

Since Eq. (5.2) is an asymptotic solution for large $\hat{r}$ (or large $\tau_{s1}\hat{r}=r\lambda_{j1}^{-1}$), then, in the context of the "generalized radiation model" of Ref. 21, this solution extends into the far precursor where the two-step ionization mechanism is dominant. Therefore, Eq. (5.2) will not provide an accurate numerical value for α for sufficiently large $\hat{r}$. It gives only the contribution of one-step ionization plus the effects of the shock wave geometry at large distances.

VI. Numerical Results

The choice of appropriate conditions for illustrative examples is guided by the following: 1) flow conditions should be close to those of Ref. 21 in order to maintain the thin collisional boundary layer and the BSE model for the tail shock structure; 2) conditions amenable to experimental verification for flat or rounded-nose bodies[26,27] are desirable; 3) the "sizing" (by choice of τ_{s1}) of the shock wave and associated body is necessary to prevent the body surface from cutting off the tail of the shock structure, etc. Argon is the monatomic gas chosen for the numerical results. Complete calculations were carried out for only one set of flow conditions because of the large amount of computer time needed to get the precursor ionization patterns on the Brown University IBM 360-Model 50 computer (7 hrs of computer time for the results presented). Items 1 and 2 are satisfied by choosing the flow conditions $p_1=10^{-3}$ atm, $T_1=300°$K and $\alpha_4(\beta=90°)=0.8$, where $\alpha_4(\beta=90°)$ is the downstream degree of ionization of the equilibrium shock on the stagnation streamline corresponding to $\hat{T}_4(\beta=90°)$.

In Fig. 5 the local downstream equilibrium shock temperature $\hat{T}_4$ and $\exp(-\hat{T}_4^{-1})$ are plotted vs angle for the flow conditions specified; since the radiation emitted from the embedded shock at each frequency is $\propto\hat{B}_\nu(\hat{T}_4)$, the decay in radiative strength with angle is $\propto\exp(-\hat{T}_4^{-1})$. In Fig. 6 the degree of ionization along the shock axis ($\theta=0$) is plotted vs the optical coordinate x/λ_{j1} for various values of

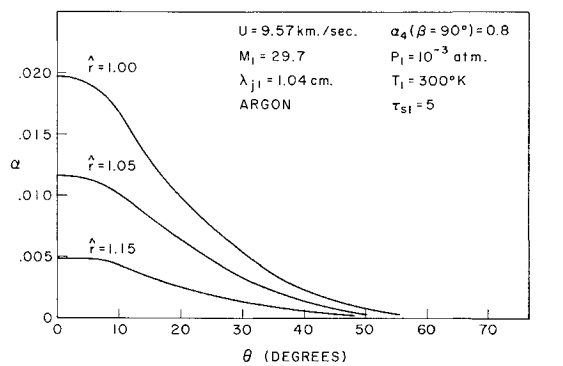

Fig. 7 Degree of ionization α vs angle θ in precursor.

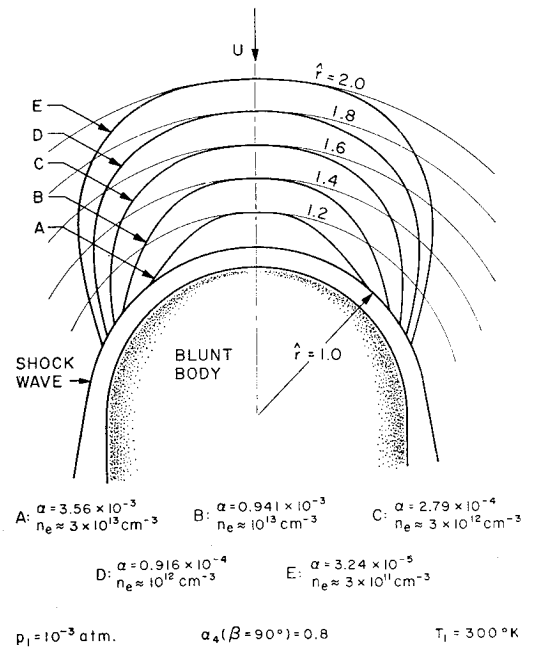

Fig. 8 Precursor radiative ionization patterns for α and n_e with $\tau_{s1} = 5$.

τ_{s1}. For $\tau_{s1} > 20$, the one-dimensional results of Ref. 16 are sensibly duplicated so that a slab model for the shock layer is then adequate for obtaining results along the stagnation streamline out to a few photon mean free paths. It is evident that a decrease in τ_{s1} increases the effects of interest herein, viz. the geometric attenuation and the associated drop in downstream shock temperature. However, $\tau_{s1} = 5$ is about as low a τ_{s1} as one would care to select in view of the sizing restrictions cited as item 3 previously. Since $\lambda_{j1} = 1.04$ cm, this gives $r_s = 5.20$ cm and a shock detachment distance of approximately 1.6 λ_{j4} at $\beta = 90°$. If the corresponding body shape were a flat-nosed cylinder, its radius would be 0.90 cm. For a hemisphere-cylinder the body radius would be approximately 4.75 cm.

The decay with angle of the degree of ionization at various values of $\hat{r}$ is shown in Fig. 7 for $\tau_{s1} = 5$. It should be noted that at $\theta \approx 50°$, α in the precursor at the embedded shock ($\hat{r} = 1$) $\approx 10^{-3}$. For larger θ there will not be sufficient precursor ionization to trigger the rapid electron-atom collisions behind the shock, and the macroscopic model of Ref. 21 will fail. However, from Fig. 5 the shock becomes radiatively weak at angles much less than 50°, but remains gas dynamically strong. Therefore, the normal shock morphology of Ref. 21 is adequate for the radiatively active portion of the present shock structure.

It is observed in Fig. 7 that as $\hat{r}$ increases, a region of constant α for given $\hat{r}$ is developing close to the shock axis for $\theta = 0 - 10°$. This phenomenon appears in the patterns formed by the curves of constant α in the precursor plasma: a complete pattern out to $\hat{r} = 2$ is shown in Fig. 8. The lettered curves are lines of constant degree of ionization α or electron density n_e. Close to the axis of symmetry, α is sensibly independent of angle for a 20° arc (10° on either side of the axis). Near the shock surface this constancy is followed by a rapid decrease in α with increase in angle while farther out the decrease in α with angle is less pronounced. Thus, the constant ionization surfaces coincide geometrically with a spherical cap at every intersection with the 10° half-angle cone specified by the $\theta = 0$ axis and the vertex at O. This "concentric sphericity effect" in the ionization near the axis can be traced to two causes, thermal and geometrical. First it can be argued that, since the downstream shock temperature does not decrease significantly between $\theta = 0 -$ 20° (this is the region where most of the radiation that influences points along the stagnation streamline comes from), then no sensible change of α with θ should be expected. However, if this were the only cause, then this "sphericity effect" should also be found in the precursor patterns for

$$-\int_1^\infty \hat{\nu}^{-1}\hat{\nabla}\cdot\hat{\mathbf{F}}_\nu d\hat{\nu}$$

From such patterns, presented in Fig. 9, it is seen that no sphericity effect occurs near the axis for $\hat{r}$ near 1; farther out, however, the radiation from the shock surface spreads out and close to the axis there is no significant change in the quantity with angle. In the vicinity of the shock surface, the cause of the sphericity effect in the ionization patterns near the axis is thus primarily geometrical. Equation (4.2) is expressible in the form

$$\alpha \propto \int_{\hat{r}}^\infty G(\hat{r},\eta,\theta)\int_1^\infty \hat{\nu}^{-1}\hat{\nabla}\cdot\hat{\mathbf{F}}_\nu d\hat{\nu}d\eta \qquad (6.1)$$

where

$$G(\hat{r},\eta,\theta) = (1 - \hat{r}^2\eta^{-2}\sin^2\theta)^{-1/2}$$

and emerges from the steady flow streamline integration. At the lower limit $\hat{r} = \eta$, the geometrical factor $G(\hat{r},\eta,\theta)$ behaves like $(\cos\theta)^{-1}$. Therefore, near $\theta = 0$, the geometric factor tends to enhance the angular independence of the degree of ionization. Thus, in the vicinity of the shock surface it is the geometry associated with the streamline integration that promotes the angular independence of α near the stagnation streamline. However, when $\theta > 10°$, the cooling of the BSE along with the line-of-sight behavior of the radiation rapidly decreases the number of electrons produced.

The numerical value of the degree of ionization obtained will not be significant physically for $\hat{r} > 2$. From Murty's criterion,[17] the two-step ionization mechanism becomes the dominant mechanism for producing electrons for the conditions studied at distances $> 10\lambda_{j1}$; this corresponds to $\hat{r} > 3$. In addition, the threshold for microwave detection devices seems to be $n_e \approx 10^{11}$ to 10^{12} cm^{-3}; this corresponds to $\hat{r} \approx 2$ for the conditions studied. The asymptotic results

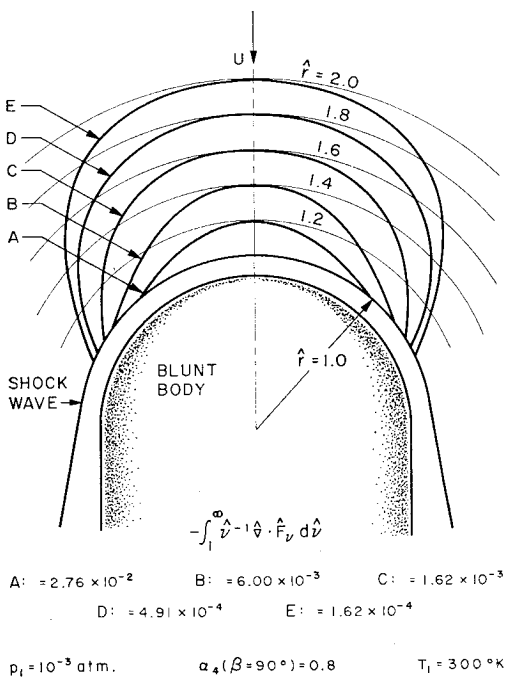

Fig. 9 Precursor patterns for $-\int_1^\infty \hat{\nu}^{-1}\hat{\nabla}\cdot\hat{F}_\nu d\hat{\nu}$ with $\tau_{s1} = 5$.

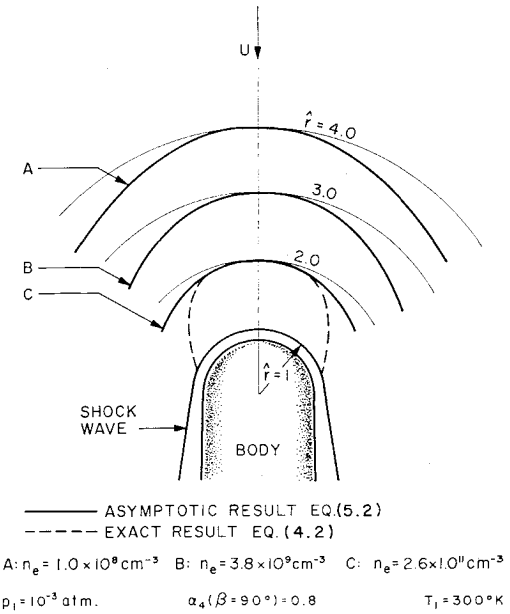

Fig. 10 Precursor ionization patterns at large distances with $\tau_{s1} = 5$.

obtained from Eq. (5.2) are presented in Fig. 10 for the constant n_e patterns at the distances $\hat{r} > 2$. For the innermost curve beginning at $\hat{r} = 2$ and for $\theta > 25°$, the asymptotic result shown is unable to reproduce the exact result shown with the broken line and obtained from Eq. (4.2). Thus, a description of the shock layer by a modified radiation point source is inappropriate for $\hat{r} \leq 2$. A source cannot describe the geometrical, thermal, and line-of-sight behavior of the radiative transfer when the influenced point is at an appropriate distance from the shock surface.

Although the results presented above are for a monatomic gas, the two geometrical phenomena associated with the multidimensionality of the problem will not be altered qualitatively by a change of gas. However, whether or not the physical description of the shock wave and shock layer is appropriate for air and other gases must be determined for those conditions of interest.

References

[1] Hollyer, R. N., Jr., "Preliminary Studies in the A.P.L. High Temperature Shock Tube," CM-903, May 1957, Johns Hopkins Univ., Applied Physics Lab.

[2] Weymann, H. D., "Electron Diffusion Ahead of Shock Waves in Argon," *The Physics of Fluids*, Vol. 3, No. 4, July-Aug. 1960, pp. 545–548.

[3] Gloersen, P., "Some Unexpected Results of Shock-Heating Xenon," *The Physics of Fluids*, Vol. 3, No. 6, Nov.-Dec., 1960, pp. 857–870.

[4] Zivanovic, S., "Investigation of Precursor Ionization in Front of Shock Waves of Hypersonic Projectiles," TR 63-2178, 1963, General Motors Defense Research Labs.

[5] Weymann, H. D. and Holmes, L. B., "Precursor Ahead of Pressure Driven Shock Waves in Argon," *Proceedings of the VIth International Conference on Ionization Phenomena in Gases*, Paris, 1962.

[6] Holmes, L. B., "Plasma Density Ahead of Pressure Driven Shock Waves," AFOSR 65-0974, TN 1, 1965, Dept. of Mechanical and Aerospace Sciences, Univ. of Rochester.

[7] Lederman, S. and Wilson, D. S. "Microwave Resonant Cavity Measurement of Shock Produced Electron Precursors," *AIAA Journal*, Vol. 5, No. 1, Jan. 1967, pp. 70–78.

[8] Lin, S. C., "Radio Echoes From a Manned Satellite during Re-Entry," *Journal of Geophysical Research*, Vol. 67, No. 10, Sept. 1962, pp. 3851–3870.

[9] Marini, J. W., "On the Decrease of the Radar Cross Section of the Apollo Command Module Due to Reentry Plasma Effects," TN-D4784, Sept. 1968, NASA.

[10] Hey, J. S., Parsons, S. J. and Stewart, G. S., "Radar Observations of the Giacobinid Meteor Shower, 1946," *Monthly Notices of the Royal Astronautical Society of London*, Vol. 107, 1947, pp. 176–183.

[11] McKinley, D. W. R. and Millman, P. M., "A Phenomenological Theory of Radar Echoes from Meteors," *Proceedings of the Institute of Radio Engineers*, Vol. 37, 1949, pp. 364–375.

[12] Cook, A. F. and Hawkins, G. S., "The Meteoric Head Echo," *Smithsonian Contribution to Astrophysics*, Vol. 5, No. 1, 1960, pp. 1–7.

[13] Hammerling, P., "Ionization Effects of Precursor Radiation from Shocks in Air," RR-98, June 1960, Avco-Everett Research Lab.

[14] Ferrari, C. and Clarke, J. H., "On Photoionization Ahead of a Strong Shock Wave," *Supersonic Flow, Chemical Processes and Radiative Transfer*, Pergamon Press, New York, 1964, pp. 375–398.

[15] Wetzel, L., "Far-Flow Approximations for Precursor Ionization Profiles," *AIAA Journal*, Vol. 2, No. 7, July 1964, pp. 1208–1213.

[16] Clarke, J. H. and Ferrari, C., "Gas Dynamics with Nonequilibrium Radiative and Collisional Ionization," *The Physics of Fluids*, Vol. 8, No. 12, Dec. 1965, pp. 2121–2139.

[17] Murty, S. S. R., "Effect of Line Radiation on Precursor Ionization," *Journal of Quantitive Spectroscopy Radiative Transfer*, Vol. 8, 1968, pp. 531–554.

[18] Dobbins, R. A., "Photoexcitation and Photoionization of Argon Ahead of a Strong Shock Wave," AIAA Paper 68–666, Los Angeles, Calif. 1968.

[19] Smith, G. L., "Radiation Induced Precursor Flow Field Ahead of a Reentry Body," AIAA Paper 68–667, Los Angeles, Calif., 1968.

[20] Edwards, K. R., "Precursor Plasma Formation for Blunt Reentry Vehicles," AIAA Paper 69–718, San Francisco, Calif., 1969.

[21] Clarke, J. H. and Onorato, M., "Asymptotic Solutions of Normal Shock Waves Structured by Nonequilibrium Radiative and Collisional Ionization," Rept. NONR-562(35)/22, March 1969, Div. of Engineering, Brown Univ.

[22] Vincenti, W. G. and Kruger, Jr., C. H., *Introduction to Physical Gas Dynamics*, Wiley, New York, 1965, pp. 462–465.

[23] Pirri, A. N., "Exact and Differential Formulations for Radiative Ionization in Cold Precursor of Detached Shock," Ph.D. thesis, June 1970, Brown Univ.

[24] Garabedian, P. R., *Partial Differential Equations*, Wiley, New York, 1964, pp. 18–24.

[25] Dobbins, R. A., private communication, June 1969, Brown, Univ.

[26] Cooper, D. M., "Equilibrium Air Radiation from Shock Layers at 11.3 km/sec.," *AIAA Journal*, Vol. 4, No. 12, Dec. 1966, pp. 2125–2130.

[27] Warren, W. R. and Harris, C. J., "A Critique of High-Performance Shock Tube Driving Techniques," Aerospace Rept. TR-0066 (5240-10)-6, Sept. 1969, Aerospace Corp., San Bernardino, Calif.